Made available by Hasselt University Library in https://documentserver.uhasselt.be

Comparative study of the interface passivation properties of LiF and Al2O3 using silicon MIS capacitor

Peer-reviewed author version

PARION, Jonathan; SCAFFIDI, Romain; DUERINCKX, Filip; SIVARAMAKRISHNAN RADHAKRISHNAN, Hariharsudan; Flandre, Denis; POORTMANS, Jef & VERMANG, Bart (2024) Comparative study of the interface passivation properties of LiF and Al2O3 using silicon MIS capacitor. In: APPLIED PHYSICS LETTERS, 124 (14) (Art N° 142901).

DOI: 10.1063/5.0203484
Handle: http://hdl.handle.net/1942/42789

Comparative study of the interface passivation properties of LiF & Al_2O_3 using silicon MIS capacitor

Jonathan Parion,[1,2,a] Romain Scaffidi,[1,2,3] Filip Duerinckx,[2] Hariharsudan Sivaramakrishnan Radhakrishnan,[2] Denis Flandre,[3] Jef Poortmans,[1,4,2] and Bart Vermang[1,2]

[1] *Hasselt University, Wetenschapspark 1, 3590 Diepenbeek, Belgium*
[2] *Imec division imo-imomec and EnergyVille, Thor Park 8320, 3600 Genk, Belgium*
[3] *ICTEAM, UCLouvain, Place du Levant 3, 1348 Louvain-la-Neuve, Belgium*
[4] *ESAT, KU Leuven, Kasteelpark Arenberg 10, 3001 Leuven, Belgium*

(Dated: 21 March 2024)

Lithium fluoride (LiF) is currently a very popular dielectric material, used as passivation or transport layer in a variety of applications and especially in high-efficiency solar cells. Despite this, its conduction properties and interface behaviour with silicon remain largely unexplored. In this work, a LiF metal-insulator-semiconductor (MIS) structure is fabricated, characterized, and its properties are compared to the well-understood aluminium oxide (Al_2O_3) MIS structure. First, a higher current density in LiF compared to Al_2O_3 is highlighted, as well as its PN junction-like behaviour with n-type silicon (n-Si), being rather unconventional for a dielectric layer. CV measurements showcase the likely presence of an interface defect, causing an increase in the apparent doping and a shift in the flat-band voltage V_{FB} by $+70\,\mathrm{meV}$. This defect is found to be of the acceptor type, which renders the interface fixed charge more negative and improve the field-effect passivation in case of a negative Q_f. Finally, a density of interface states $D_{it} \approx 2 \times 10^{11}\,\mathrm{cm^{-2}eV^{-1}}$ was found for LiF/n-Si, which is a low value showing appropriate chemical passivation at the interface. Overall, this work enables to shine more light on the interface properties of LiF on n-Si, which is an essential step towards its wider use in state-of-the art solar cells and other silicon-based devices.

Lithium fluoride (LiF) was previously presented as a very good material to lower the work function of metallic electrodes in light-emitting devices, therefore improving their contact properties[1–3]. It was recently also successfully demonstrated as an efficient passivation and transport layer in state-of-the-art solar cells achieving world-record efficiencies[4–6]. Moreover, the key role played by passivation in many silicon-based devices motivates that LiF could be of great interest well beyond the LED and solar cells applications. Despite these promising aspects, the conduction and interface properties of LiF with silicon are to this day largely unexplored, which is a major bottleneck in using this material in a wider range of applications.

The objective of this work is to provide a better understanding of the interface properties of LiF on n-type silicon (n-Si), by comparing it to Al_2O_3. This choice is motivated by the excellent passivation properties of Al_2O_3 on silicon and the extensive knowledge gathered for this material, especially in the context of silicon solar cells. For this comparison, the well-known metal-insulator-semiconductor (MIS) architecture is used, as schematically represented in Fig. 1. For the LiF MIS, a n-type silicon wafer with resistivity $\rho \approx 2\,\Omega\mathrm{cm}$ is used, similarly to state-of-the-art silicon solar cells. The wafer is cleaned following a standard process and a 20nm layer of LiF is thermally evaporated on top. The front contact is achieved using a mercury (Hg) probe station. Aluminium is evaporated on the backside of the wafer to create an ohmic contact. The same procedure is followed for the Al_2O_3 MIS, but with 20nm of Al_2O_3 deposited on top of n-Si by thermal atomic layer deposition.

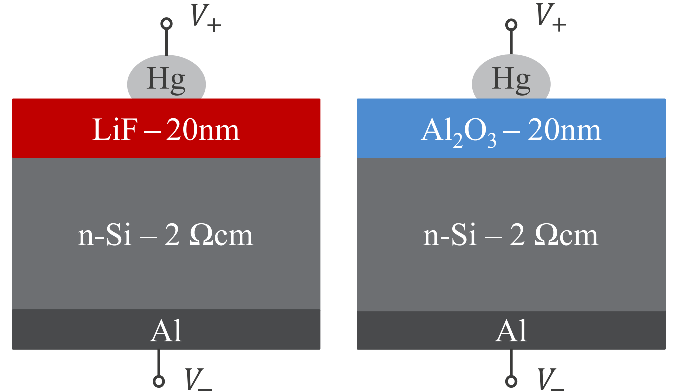

FIG. 1. Schematic representation of the devices used in this work. The front Hg contact (at the top) is realized with a mercury probe station, in which and liquid mercury is brought in contact with the sample during the measurement and removed afterwards. This takes place under vacuum and enables to achieve optimal contact, without damaging the dielectric layer. The device active area is $A = 0.0065\,\mathrm{cm}^2$.

First, current-voltage (IV) measurements are realized in the dark to assess the conduction properties of both materials. Then, capacitance-voltage (CV) and conductance-voltage (GV) measurements are performed, also in the dark, to extract the interface and passivation properties of both materials.

IV measurements are carried out in the dark, using a Keithley 2401 sourcemeter. Positive voltage is applied

[a] jonathan.parion@hotmail.be

at the front, as shown in Fig. 1. The experimental JV characteristics of both Al_2O_3 and LiF MIS stacks are represented in Fig. 2.

The current density in a MIS structure with a conventional dielectric is expected to be very low due to the wide bandgap of the material. It is dominated by ohmic conduction at low and reverse voltage biases, and by tunnelling currents in larger forward bias. Typically, currents of the order of $10^{-5} - 10^{-3}\,\mathrm{mA/cm^2}$ can be observed in Al_2O_3/Si MIS capacitors, under 1V voltage bias, depending on the film thickness and the deposition process[7,8]. This appears to be in line with the observations in Fig. 2, where the current density for Al_2O_3 is about $3 \times 10^{-4}\,\mathrm{mA/cm^2}$ at 1V. The low current density explains why Al_2O_3 transport layers are either very thin[9,10] or thicker and porous[11,12], so as to not significantly hinder the transport of charge carriers. This requirement is however not necessary when Al_2O_3 is used as passivation layer, since the current does not directly flow through the layer itself[13,14].

Compared to Al_2O_3, the current density for the LiF MIS displayed in Fig. 2 is noticeably higher, with a value of $2 \times 10^{-3}\,\mathrm{mA/cm^2}$ at 1V. This could seem surprising, as the layers thicknesses are similar, and the bandgap of LiF ($E_g = 13\,\mathrm{eV}$) is far greater than the one of Al_2O_3 ($E_g = 6.2\,\mathrm{eV}$). However, such high current density in thick LiF layers was previously reported[15], and might be related to hopping conduction, in which carriers tunnel through defect states present in the dielectric film[16]. These conduction properties were also observed in thinner films[1–3] and should be, as mentioned earlier, beneficial in the case of a transport layer.

Conventional dielectrics such as Al_2O_3 are in essence intrinsic layers, without any form of doping. In LiF on the contrary, the alleged bulk trap states might act as doping elements in the layer, therefore stepping away from the expected dielectric behaviour. This hypothesis seems to be confirmed by the shape of the curve in Fig. 2, where LiF exhibits a very typical PN junction characteristic. The current density increases exponentially around 0V and is negative in reverse bias, as clearly shown in the inset of Fig. 2. Also in reverse bias, the current is linear with respect to voltage with a steep decrease. This indicates a large minority carriers leakage current that is not observed for Al_2O_3, and might arguably have different contributions. Indeed, the possible presence of shunt paths in the LiF layer caused by localized pinholes, likely not present for the conformal ALD Al2O3 layer, or the impact of the LiF intrinsic doping may play a role, among others. This would require further investigations but is not considered to impede the presented analysis in the bias range of interest. The fact that LiF does not behave as a real dielectric but rather as a doped semiconductor layer is a first important sign of its unconventional properties, and is taken into account when trying to apply the classical MIS theory in the following.

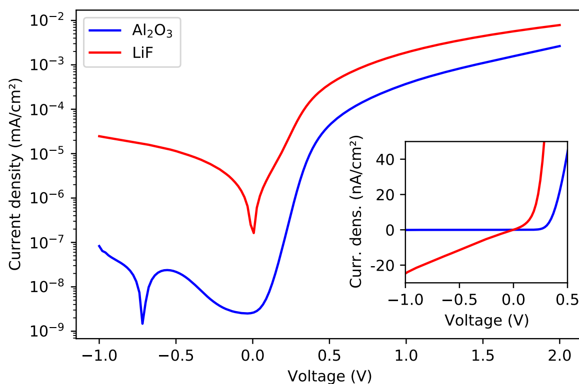

FIG. 2. Experimental current density characteristic for both Al_2O_3 and LiF structures, presented in logarithmic scale. The behaviour of these structures is represented in linear scale in the inset, highlighting the diode behaviour of LiF more clearly.

Interface properties of LiF and Al_2O_3 are extracted using CV and GV measurements. These are conducted using an HP 4284A LCR meter, with positive voltage applied on the front contact (Fig. 1). The measurements are performed at 10 kHz, with a varying voltage between −0.5 V and 2 V. Following the well-established theory of MIS capacitors[17], the flat-band voltage (V_{FB}) of the structure can be expressed as:

$$\frac{V_{FB}}{q} = \phi_{ms} - \frac{Q_f}{C_{ox}} \quad (1)$$

with ϕ_{ms} the contact potential difference, Q_f the fixed charge at the dielectric interface, C_{ox} the dielectric capacitance and q the elementary charge. In an ideal case where there is no interface charge, $q\phi_{ms} = V_{FB}$. In the presence of a fixed charge at the interface, the value of V_{FB} becomes greater or smaller if the charge sign is respectively negative or positive, corresponding to a shift of the CV characteristic in the rightward or leftward direction[17]. In an uniformly doped substrate, the experimental value of V_{FB} is extracted by taking the intercept between the horizontal axis and the linear region of the C^{-2} vs V plot[18]. The value of the apparent doping (N_D) is also extracted from the slope of that linear region, following:

$$N_D = \frac{2}{q\varepsilon_r\varepsilon_0} \times \left(|slope|A^2\right) \quad (2)$$

with ε_r the electrical permittivity of the semiconductor, ε_0 the electrical permittivity of vacuum and A the gate area. The values of both V_{FB} and N_D were obtained for Al_2O_3 and LiF from the experimental CV data and are presented in Fig. 3.

The CV characteristic of the Al_2O_3 device, shown in the inset of Fig. 3, depicts the typical behaviour of n-type MIS capacitors with the accumulation region beyond 1V and the depletion regime for negative or low forward bias.

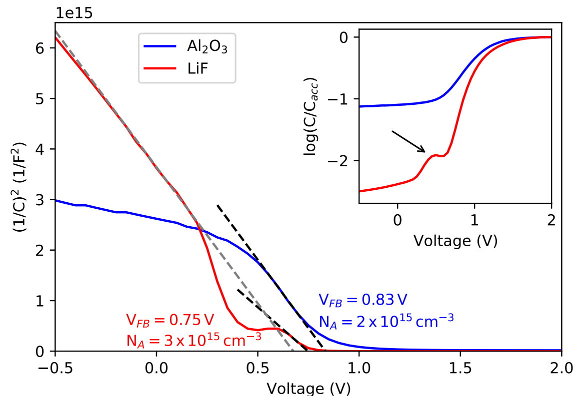

FIG. 3. Experimental C^{-2} vs V plot, obtained from CV measurements at 10kHz. V_{FB} is extracted by extrapolation of the linear region of the C^{-2} vs V curve to the x-axis (black dashed lines). An additional line is represented in gray for LiF, to highlight the impact of the interface defect on V_{FB}. The normalized CV characteristic of both stacks is represented in log-scale in the top-right inset, and the response due to the interface defect identified for LiF is pointed with a black arrow.

The value of apparent doping $N_D = 2 \times 10^{15}\,\text{cm}^{-3}$ extracted from the C^{-2} vs V characteristic (Fig. 3) comes rather close to the estimation $N_{D,th.} = 2.3 \times 10^{15}\,\text{cm}^{-3}$ based on the wafer resistivity $\rho_s \approx 2\,\Omega\text{cm}$, which tends to confirm the applicability of the model for the Al_2O_3 structure. Subsequently, a value of flat-band voltage $V_{FB} = 0.83\,\text{V}$ is obtained for Al_2O_3.

In the inset of Fig. 3, it appears that the CV characteristic of the LiF device also presents two distinct regions similarly to the Al_2O_3 structure. However, it exhibits a noticeable difference around 0.5 V where the LiF curve shows a distinct peak emphasized by a black arrow. This feature is most probably originating from an electronic defect[19–21]. When the applied voltage bias is varied, the position of the Fermi level in the bandgap changes, resulting in defects states being charged and discharged. In function of the defect type (bulk, interface) and its properties (activation energy, capture cross-section), it contributes to the total measured capacitance of the device in a particular range of voltages. Interface defects in particular have a very limited span in terms of energy levels, and therefore charge and discharge themselves for a limited range of voltages. This results in a narrow response in the CV plot, which is visibly the case in Fig. 3. This tends to indicate that the electronic defect is in fact an interface defect, most probably located at the interface between LiF and n-Si. It should be carefully considered when experimentally extracting the interface parameters, as it will likely influence the total charge and thus N_D, Q_f and V_{FB}.

The interface defect produces a different pattern on the C^{-2} vs V characteristic, positioned around the same 0.5 V bias. Contrarily to Al_2O_3, there are actually two distinct linear regions for LiF, yielding different values of N_D and V_{FB}. The first one occurs before 0.4 V (gray dashed line - region 1) and the second one around $0.7 - 0.8\,\text{V}$ (black dashed line - region 2), leading to $N_D = 2 \times 10^{15}\,\text{cm}^{-3}$ and $N_D = 3 \times 10^{15}\,\text{cm}^{-3}$ respectively. The value for N_D in region 1 is similar to the one obtained for Al_2O_3 (parallel intercept lines) and therefore also to the theoretical doping of the wafer. This tends to indicate that the defect state would be depleted before 0.5V and filled with charges after that, therefore contributing to the total apparent doping that is higher in region 2. Region 1 would therefore be related to the intrinsic "defect-free" interface behaviour between LiF and n-Si and region 2 to a combination of both the intrinsic and interface defect contributions.

Due to the interface defect, there is a difference of +70 meV between the V_{FB} value that would be extracted in region 1 ($V_{FB} = 0.63\,\text{V}$) and in region 2 ($V_{FB} = 0.75\,\text{V}$). Following Eq. 1, an increase in V_{FB} within a single structure where ϕ_{ms} and C_{ox} are constant is necessarily caused by a more negative Q_f. This suggests that the additional charge generated by the interface defect states is negative, therefore pointing towards an acceptor-type defect.

When investigating the passivation properties of a dielectric material, two distinct mechanisms are considered. The first one is usually related to the fixed charge at the interface between the dielectric and the n-Si substrate (Q_f) and is called field-effect passivation[17,22,23]. Its magnitude and sign (positive or negative) depend on the interface defect density and type (donor or acceptor), respectively. Q_f is obtained as[17]:

$$Q_f = C_{ox} \times \left(\frac{V_{ms} - V_{FB}}{q} \right) \tag{3}$$

where $V_{ms} = q\phi_{ms}$. This equation is derived from Eq. 1 and is valid in the case of traditional dielectrics. For experimental data, V_{FB} is obtained as described in the previous section, C_{ox} is extracted experimentally in the accumulation regime and V_{ms} is computed as:

$$V_{ms} = V_m - \frac{1}{q} \left(\xi_{Si} + \frac{E_{g,Si}}{2} - (kT) \ln \left(\frac{N_D}{n_i} \right) \right) \tag{4}$$

where $V_m = 4.45\,\text{V}$ is the work function of the mercury probe, $\xi_{Si} = 4.05\,\text{eV}$ is the n-Si electron affinity, $E_{g,Si} = 1.12\,\text{eV}$ is the n-Si bandgap, $kT/q = 0.026\,\text{eV}$ is the thermal energy and $n_i \approx 1.5 \times 10^{10}\,\text{cm}^{-3}$ is the intrinsic density of carriers in n-Si at room temperature[24]. Based on the previous computation and in the case of Al_2O_3, the interface fixed charge is $Q_f = -2.3 \times 10^{12}\,\text{cm}^{-2}$, as also obtained in similar studies[22,23,25]. A negative fixed charge for a dielectric on a n-type Si wafer is useful at the low-potential side, since it facilitates the extraction of positive charge carriers (holes) when used as a transport layer.

The same methodology is not directly applicable for LiF, since it does not behave as an ideal dielectric in the

same way as Al_2O_3 does. Due to its PN junction-like behaviour with n-Si, it is not possible to accurately extract a value for Q_f. More precisely, the possible doping of the LiF layer introduces additional charges, which also influence the experimental Q_f value. This should however be confirmed by further investigation on the LiF layer itself, which is outside the scope of this work. Despite these uncertainties, it was previously shown that the interface defect is of acceptor type, therefore adding a negative charge to the interface. Depending on the "intrinsic" value of Q_f, this can either increase the field-effect passivation ($Q_f < 0$) or decrease it ($Q_f > 0$). Based on the similarities between Al_2O_3 and LiF in terms of V_{FB}, it is reasonable to think that if $Q_{f,\mathrm{Al_2O_3}}$ is negative, so will be $Q_{f,\mathrm{LiF}}$. In that case, the interface defect actually strengthens the field-effect passivation, which is a beneficial feature of that defect.

The second passivation mechanism is related to the density of electronic defects at the n-Si interface (D_{it}) and is called chemical passivation[17,22,23]. Using Al_2O_3 to passivate the interface between n-Si and the neighbouring electrical contact is greatly motivated by the subsequent reduction of D_{it} by one or even two orders of magnitude. A well-established technique to experimentally extract D_{it} is the conductance technique[17]. It is based on the evolution of the parallel conductance with voltage and frequency, which is obtained as:

$$\frac{G_p}{A\omega} = \frac{\omega G_m C_m^2}{G_m^2 + (\omega C_m)^2} \tag{5}$$

with $\omega = 2\pi f$ the angular frequency, C_m the measured capacitance and G_m the measured conductance that are both normalised by the area of the device. The capture and emission of charges by interface traps lead to a certain energy loss, which can be modelled by $G_p/A\omega$[8]. A peak in $G_p/A\omega$ with respect to voltage and frequency indicates the crossing of a defect state by the Fermi level in the same way as for the capacitance, both quantities being mathematically linked[26]. Based on this, the value of D_{it} can therefore be obtained by looking at the response peak, using[17]:

$$D_{it} = 2.5 \times \left(\frac{G_p/A\omega}{q}\right)_{\max} \tag{6}$$

The $G_p/A\omega$ vs V characteristic is represented in Fig. 4.

The most significant feature appearing in the $G_p/A\omega$ characteristic is the peak in conductance around 0.4 V in the LiF curve, which is likely caused by the interface defect identified before. At that voltage bias, the $G_p/A\omega$ response is about one order of magnitude greater for LiF than for Al_2O_3. It would be fair to question whether it is possible to compute a real value of D_{it} using $G_p/A\omega$, since it was previously shown to not behave as a real dielectric but rather as a PN junction. Several studies have previously used the conductance technique in MIS structures using non-conventional dielectrics and in PN

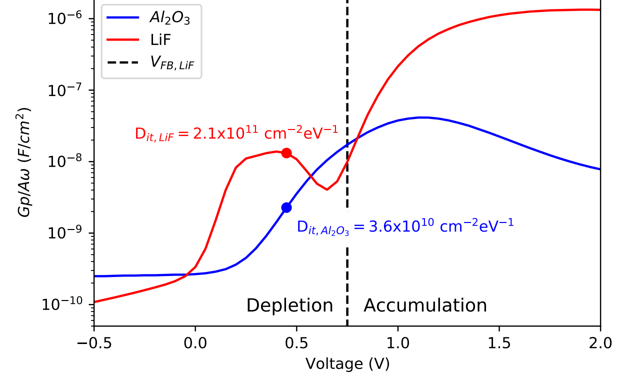

FIG. 4. Experimental $G_p/A\omega$ vs V plot, obtained from GV measurements at 10kHz. The limit between the depletion and accumulation regime is represented for LiF. D_{it} is extracted in depletion for both dielectrics and represented on the figure.

junctions to extract D_{it}[23,27–29]. An important condition to this is that the D_{it} extraction is only valid in the depletion regime (low voltage bias) and not in accumulation where the conductance value might be altered by the large DC current. In Fig. 4, the separation ($V = V_{FB}$) between depletion and accumulation for LiF is clearly demarcated by a black dashed line. In a similar fashion, when the reverse leakage current is high, care must also be taken on the interpretability of the results for negative voltage bias. The response for G_p/ω in reverse bias in Fig. 4 is not flat for LiF, contrarily to Al_2O_3, which is probably caused by the large reverse leakage current that was highlighted in the inset of Fig. 2. All in all, because the peak in conductance for LiF is situated in depletion regime, it is fair to assume that a plausible value of D_{it} can indeed be extracted, being $D_{it} \approx 2 \times 10^{11}\,\mathrm{cm^{-2}eV^{-1}}$. This is lower than for a direct electrical contact on silicon, therefore showing the good passivation properties of LiF. In the Al_2O_3 device at the same voltage bias, $D_{it} \approx 4 \times 10^{10}\,\mathrm{cm^{-2}eV^{-1}}$. The value of D_{it} is in this case not extracted at the peak position in voltage, because it is situated in accumulation which does not satisfy the assumptions of Eq. 6. Moreover, the reported value is very close to the one reported in similar studies[22,23,25], which justifies that it could constitute a good comparison point for the preceding analysis.

In this work, the interface passivation properties of LiF on n-Si are investigated, and compared to those of Al_2O_3 using the well-known MIS architecture.

JV measurements show a current density of $2 \times 10^{-3}\,\mathrm{mA/cm^2}$ at 1V for LiF, which is about 1 order of magnitude higher than for Al_2O_3 and constitute a real asset if LiF were to be used as a charge transport layer. These measurements also highlighted the unconventional dielectric behaviour of LiF on n-Si, which is closer to the one of a PN junction and might be explained by a high

doping in the LiF layer.

Using CV measurements, the likely presence of an acceptor-type interface defect is identified, which results in an increase of the apparent doping from $N_D = 2\times10^{15}\,\mathrm{cm}^{-3}$ to $N_D = 3\times10^{15}\,\mathrm{cm}^{-3}$ as well as in a rightwards shift of V_{FB} by 70 meV. Moreover, this interface defect was proven to make the interface fixed charge more negative, which in the case of a negative Q_f strengthens the field-effect passivation.

Finally, GV measurements and the associated $G_p/A\omega$ characteristics enable to extract an interface trap density value $D_{it} \approx 2\times10^{11}\,\mathrm{cm}^{-2}\mathrm{eV}^{-1}$, which is about one order of magnitude greater than Al_2O_3 at the same voltage bias, but still very low to show good chemical passivation properties.

Overall, the comparison made in this work highlights the peculiar properties of LiF on n-Si, compared to those of Al_2O_3. This should enable a better understanding of the material and its properties, therefore contributing to its wider adoption as transport layer in n-type silicon solar cells but also in other silicon-based devices.

The authors thank the teams of the nanofabrication shared facility (WINFAB) and electrical characterization platform (WELCOME) at UCLouvain for their availability and technical support.

The data that support the findings of this study are available from the corresponding author upon reasonable request.

[1] M. G. Mason, C. W. Tang, L.-S. Hung, P. Raychaudhuri, J. Madathil, D. J. Giesen, L. Yan, Q. T. Le, Y. Gao, S.-T. Lee, L. S. Liao, L. F. Cheng, W. R. Salaneck, D. A. dos Santos, and J. L. Brédas, "Interfacial chemistry of Alq3 and LiF with reactive metals," Journal of Applied Physics **89**, 2756–2765 (2001).

[2] T. M. Brown, R. H. Friend, I. S. Millard, D. J. Lacey, J. H. Burroughes, and F. Cacialli, "Efficient electron injection in blue-emitting polymer light-emitting diodes with LiF/Ca/Al cathodes," Applied Physics Letters **79**, 174–176 (2001).

[3] T. M. Brown, R. H. Friend, I. S. Millard, D. J. Lacey, T. Butler, J. H. Burroughes, and F. Cacialli, "Electronic line-up in light-emitting diodes with alkali-halide/metal cathodes," Journal of Applied Physics **93**, 6159–6172 (2003).

[4] D. Menzel, A. Al-Ashouri, A. Tejada, I. Levine, J. A. Guerra, B. Rech, S. Albrecht, and L. Korte, "Field effect passivation in perovskite solar cells by a LiF interlayer," Advanced Energy Materials **12**, 2201109 (2022), https://onlinelibrary.wiley.com/doi/pdf/10.1002/aenm.202201109.

[5] A. Al-Ashouri, E. Köhnen, B. Li, A. Magomedov, H. Hempel, P. Caprioglio, J. A. Márquez, A. B. M. Vilches, E. Kasparavicius, J. A. Smith, N. Phung, D. Menzel, M. Grischek, L. Kegelmann, D. Skroblin, C. Gollwitzer, T. Malinauskas, M. Jošt, G. Matič, B. Rech, R. Schlatmann, M. Topič, L. Korte, A. Abate, B. Stannowski, D. Neher, M. Stolterfoht, T. Unold, V. Getautis, and S. Albrecht, "Monolithic perovskite/silicon tandem solar cell with 29% efficiency by enhanced hole extraction," Science **370**, 1300–1309 (2020), https://www.science.org/doi/pdf/10.1126/science.abd4016.

[6] M. Q. Khokhar, S. Q. Hussain, D. P. Pham, S. Lee, H. Park, Y. Kim, E.-C. Cho, and J. Yi, "Simulation of Silicon Heterojunction Solar Cells for High Efficiency with Lithium Fluoride Electron Carrier Selective Layer," Energies **13**, 1635 (2020).

[7] J. Kolodzey, E. Chowdhury, T. Adam, G. Qui, I. Rau, J. Olowolafe, J. Suehle, and Y. Chen, "Electrical conduction and dielectric breakdown in aluminum oxide insulators on silicon," IEEE Transactions on Electron Devices **47**, 121–128 (2000).

[8] Y. Yan, V. Kilchytska, B. Wang, S. Faniel, Y. Zeng, J.-P. Raskin, and D. Flandre, "Characterization of thin Al2O3/SiO2 dielectric stack for CMOS transistors," Microelectronic Engineering **254**, 111708 (2022).

[9] J. Deckers, E. Cornagliotti, M. Debucquoy, I. Gordon, R. Mertens, and J. Poortmans, "Aluminum Oxide-aluminum Stacks for Contact Passivation in Silicon Solar Cells," Energy Procedia Proceedings of the 4th International Conference on Crystalline Silicon Photovoltaics (SiliconPV 2014), **55**, 656–664 (2014).

[10] J. De Wild, G. Birant, G. Brammertz, M. Meuris, J. Poortmans, and B. Vermang, "Ultrathin Cu(In,Ga)Se-2 Solar Cells with Ag/AlOx Passivating Back Reflector," (2021), 10.3390/en14144268, accepted: 2021-12-06T10:53:58Z Publisher: MDPI.

[11] I. Kandybka, G. Birant, J. De Wild, D. Buldu Kohl, T. Kohl, R. Thiruvallur Eachambadi, G. Brammertz, J. Manca, M. Meuris, J. Poortmans, and B. Vermang, "Novel cost-effective approach to produce nano-sized contact openings in an aluminum oxide passivation layer up to 30 nm thick for CIGS solar cells," (2021).

[12] D. Buldu, J. De Wild, T. Kohl, G. Birant, G. Brammertz, M. Meuris, J. Poortmans, and B. Vermang, "A Novel Strategy for the Application of an Oxide Layer to the Front Interface of Cu(In,Ga)Se2 Thin Film Solar Cells: Al2O3/HfO2 Multi-Stack Design With Contact Openings," (2022), 10.1109/JPHOTOV.2021.3120515.

[13] B. Vermang, H. Goverde, L. Tous, A. Lorenz, P. Choulat, J. Horzel, J. John, J. Poortmans, and R. Mertens, "Approach for Al2O3 rear surface passivation of industrial p-type Si PERC above 19%," Progress in Photovoltaics: Research and Applications **20**, 269–273 (2012), https://onlinelibrary.wiley.com/doi/pdf/10.1002/pip.2196.

[14] S. Banerjee and M. K. Das, "A review of Al2O3 as surface passivation material with relevant process technologies on c-Si solar cell," Optical and Quantum Electronics **53**, 60 (2021).

[15] B. F. Bory, H. L. Gomes, R. A. J. Janssen, D. M. de Leeuw, and S. C. J. Meskers, "Electrical conduction of LiF interlayers in organic diodes," Journal of Applied Physics **117**, 155502 (2015).

[16] F.-C. Chiu, "A Review on Conduction Mechanisms in Dielectric Films," Advances in Materials Science and Engineering **2014**, 1–18 (2014).

[17] E. H. Nicollian and J. R. Brews, *MOS (Metal Oxide Semiconductor) Physics and Technology* (John Wiley and Sons, 1982).

[18] K. Piskorski and H. M. Przewlocki, "The methods to determine flat-band voltage VFB in semiconductor of a MOS structure," in *The 33rd International Convention MIPRO* (2010) pp. 37–42.

[19] G. Brammertz, T. Kohl, J. de Wild, D. G. Buldu, G. Birant, M. Meuris, J. Poortmans, and B. Vermang, "Bias-dependent admittance spectroscopy of thin-film solar cells: Experiment and simulation," IEEE Journal of Photovoltaics **10**, 1102–1111 (2020).

[20] J. Parion, R. Scaffidi, D. Flandre, G. Brammertz, and B. Vermang, "Low-temperature admittance spectroscopy for defect characterization in Cu(In,Ga)(S,Se)2 thin-film solar cells," in *IEEE EUROCON 2023 - 20th International Conference on Smart Technologies* (2023) pp. 99–104.

[21] J. Parion, "Opto-electrical characterization and modelling of defects in thin-film Cu(In,Ga)Se2 solar cells," (2022).

[22] R. Kotipalli, R. Delamare, O. Poncelet, X. Tang, L. A. Francis, and D. Flandre, "Passivation effects of atomic-layer-deposited aluminum oxide," EPJ Photovoltaics **4**, 45107 (2013).

[23] R. Scaffidi, D. G. Buldu, G. Brammertz, J. de Wild, T. Kohl, G. Birant, M. Meuris, J. Poortmans, D. Flandre, and B. Vermang, "Comparative Study of Al_2O_3 and HfO_2 for Surface Passivation of $Cu(In,Ga)Se_2$ Thin Films: An Innovative

Al_2O_3/HfO_2 Multistack Design," physica status solidi (a) **218**, 2100073 (2021).

[24] S. M. Sze and K. K. Ng, *Physics of semiconductor devices*, 3rd ed. (Wiley-Interscience, Hoboken, N.J, 2007).

[25] L. Black, *New Perspectives on Surface Passivation: Understanding the Si-Al2O3 Interface*, Springer Theses, Recognizing Outstanding Ph.D. Research (Springer, Germany, 2016) doctoral Thesis accepted by the Australian National University, Australia.

[26] C. León, J. M. Martin, J. Santamaría, J. Skarp, G. González-Díaz, and F. Sánchez-Quesada, "Use of Kramers–Kronig transforms for the treatment of admittance spectroscopy data of p - n junctions containing traps," Journal of Applied Physics **79**, 7830–7836 (1996), number: 10.

[27] W. Fahrner, T. Mueller, M. Scherff, D. Knoner, and H. Neitzert, "Interface states of heterojunction solar cells," (2006) pp. 1160 – 1163.

[28] J. M. V. Cunha, M. A. Barreiros, M. A. Curado, T. S. Lopes, K. Oliveira, A. J. N. Oliveira, J. R. S. Barbosa, A. Vilanova, M. J. Brites, J. Mascarenhas, D. Flandre, A. G. Silva, P. A. Fernandes, and P. M. P. Salomé, "Perovskite metal–oxide–semiconductor structures for interface characterization," Advanced Materials Interfaces **8**, 2101004 (2021), https://onlinelibrary.wiley.com/doi/pdf/10.1002/admi.202101004.

[29] J. de Wild, R. Scaffidi, G. Brammertz, G. Birant, and B. Vermang, "Dielectric front passivation for cu(in,ga)se2 solar cells: Status and prospect," Advanced Energy and Sustainability Research **4**, 2200132 (2023), https://onlinelibrary.wiley.com/doi/pdf/10.1002/aesr.202200132.